Meteoritics 30, 57–70 (1995)

Silica-rich orthopyroxenite in the Bovedy chondrite

ALEX RUZICKA[1], DAVID A. KRING[1], DOLORES H. HILL[1], WILLIAM V. BOYNTON[1], ROBERT N. CLAYTON[2,3] AND TOSHIKO K. MAYEDA[2]

[1]Department of Planetary Sciences, University of Arizona, Tucson, Arizona 85721, USA
[2]Enrico Fermi Institute, University of Chicago, Chicago, Illinois 60637, USA
[3]Department of Chemistry, and Department of the Geophysical Sciences, University of Chicago, Chicago, Illinois 60637, USA

(Received 1994 April 15; accepted in revised form 1994 November 11)

Abstract–A large (>4.5 x 7 x 4 mm), igneous-textured clast in the Bovedy (L3) chondrite is notable for its high bulk SiO_2 content (≈57.5 wt%). The clast consists of normally zoned orthopyroxene (83.8 vol%), tridymite (6.2 %), an intergrowth of feldspar (5.8 %) and sodic glass (3.1 %), pigeonite (1.0 %), and small amounts of chromite (0.2 %), augite, and Fe,Ni-metal; it is best described as a silica-rich orthopyroxenite. The oxygen-isotopic composition of the clast is similar, but not identical, to Bovedy and other ordinary chondrites. The clast has a superchondritic Si/Mg ratio, but has Mg/(Mg + Fe) and Fe/Mn ratios that are similar to ordinary chondrite silicate. The closest chemical analogues to the clast are radial-pyroxene chondrules, diogenites, pyroxene-silica objects in ordinary chondrites, and silicates in the IIE iron meteorite Weekeroo Station.

The clast crystallized from a siliceous melt that cooled fast enough to prevent complete attainment of equilibrium but slow enough to allow nearly complete crystallization. The texture, form, size and composition of the clast suggest that it is an igneous differentiate from an asteroid or planetesimal that formed in the vicinity of ordinary chondrites. The melt probably cooled in the near-surface region of the parent object. It appears that in the source region of the clast, metallic and silicate partial melt were largely-to-completely lost during a relatively low degree of melting, and that during a higher degree of melting, olivine and low-Ca pyroxene separated from the remaining liquid, which ultimately solidified to form the clast. While these fractionation steps could not have all occurred at the same temperature, they could have been accomplished in a single melting episode, possibly as a result of heating by radionuclides or by electromagnetic induction. Fractionated magmas can also account for other Si-rich objects in chondrites.

INTRODUCTION

Igneous-textured objects larger than about 1 mm in diameter are uncommon in ordinary chondrites, and large objects poor in olivine are rarer still. One of the most striking examples of such a large, olivine-poor object is a clast of silica-rich orthopyroxenite in the Bovedy (L3) chondrite (Ruzicka and Boynton, 1992a,b; Ruzicka *et al.*, 1993), which contains a silica polymorph (probably tridymite) and no olivine.

The clast is the largest known example of a diverse collection of objects in ordinary chondrites, previously described as chondrules and clasts, that contain a silica mineral. These include pyroxene-silica objects, which are composed almost entirely of pyroxene and a silica mineral (Planner, 1983; Brigham *et al.*, 1986; Nakamura *et al.*, 1990; Krot and Wasson, 1993), fayalite-silica objects consisting primarily of a silica mineral cross-cut and rimmed by fayalitic olivine (Brigham *et al.*, 1986; Krot and Wasson, 1993; Wasson and Krot, pers. comm., 1993), and other objects that contain K-feldspar (Bischoff *et al.*, 1993; Wlotzka *et al.*, 1983). Isolated mm-to-cm-sized xenocrysts or inclusions of cristobalite and tridymite have also been found (*e.g.*, Olsen *et al.*, 1981; Ehlmann *et al.*, 1988). In addition to these objects in ordinary chondrites, two pyroxene-plagioclase-silica objects have been described from the CM chondrite Murchison (Olsen, 1983), and pyroxene-silica and pure silica objects have been found in the unusual chondrite ALH 85085 (Bischoff *et al.*, 1989).

All of the Si-rich objects in ordinary chondrites (excluding single grains of SiO_2) contain appreciable amounts of FeO, as opposed to the enstatite chondrites, which also contain silica polymorphs but are instead nearly FeO-free. While many of the silica-rich objects have irregular margins and appear to be fragments of larger objects, some have curved outlines and appear to be drop-formed (including some pyroxene-silica objects and the two Murchison objects).

Given the variety of Si-rich objects in ordinary and carbonaceous chondrites, it is perhaps unsurprising that the proposed origins for them are equally diverse. These include: (1) extreme reduction of chondritic material (Brigham *et al.*, 1986); (2) melting of vapor-solid fractionated nebular materials, either in the nebula (Brigham *et al.*, 1986) or on a parent body (Nakamura *et al.*, 1990); (3) collision-induced mixing or melt phase separation (Brigham *et al.*, 1986; Nakamura *et al.*, 1990); (4) parent body or nebular alteration of one type of silica-rich object (pyroxene-silica) to form another type (fayalite-silica) (Krot and Wasson, 1993; Wasson and Krot, pers. comm., 1993); (5) shock melting of chondritic material either preceded or accompanied by vapor-solid exchange with surrounding hot gases (Wlotzka *et al.*, 1983); and (6) igneous differentiation in a "planetary" (asteroidal or planetesimal) setting (Olsen, 1983; Ruzicka and Boynton, 1992a,b; Ruzicka *et al.*, 1993; Bischoff *et al.*, 1993).

This paper provides data, models and observations relating to the large Si-rich orthopyroxenite clast, designated Bo-1, in Bovedy. Preliminary results of our investigation were reported elsewhere (Ruzicka and Boynton, 1992a,b; Ruzicka *et al.*, 1993). The first section of this paper describes the petrography and composition of the clast, which suggests an igneous origin from material similar to, but probably distinct from, the material out of which ordinary chondrites formed. In the second section, we discuss various origins for the siliceous liquid represented by Bo-1 and conclude that it formed by igneous differentiation. A similar origin was previously proposed for other large objects in ordinary chondrites, including a 2-mm-diameter glass bleb in Bovedy (Graham *et al.*,

1976), a 15 x 12 x 12 mm-diameter troctolitic pebble in Barwell (Hutchison *et al.*, 1988), and an ≈2-mm-diameter microgabbro clast in Parnallee (Kennedy *et al.*, 1992). All of these objects are poorer in Si and more feldspathic than Bo-1.

METHODS AND SAMPLES

A slab of Bovedy containing a conspicuous light-colored object (clast) was obtained from Mr. Ronald Farrell. Bovedy is classified as an L3 chondrite on the basis of its composition, distinct chondrules, and presence of glassy mesostases within chondrules (Graham *et al.*, 1976). The meteorite was shock-metamorphosed (Graham *et al.*, 1976; Rubin *et al.*, 1981). Rubin *et al.* (1981) described a large, light-colored, igneous clast in Bovedy different from the one reported here and classified Bovedy as a fragmental breccia. Olivine in the meteorite has a rather uniform composition, unusual for a chondrite of such low textural type (Graham *et al.*, 1976), which may be the result of diffusional exchange during post-shock annealing. Bifurcating shock veins, including glassy silicate-rich veins and coarse metal- and sulfide-rich veins, traverse the host meteorite. Minor sulfide-rich shock veins cross over into the clast in a few locations.

SEM and Microprobe Studies

The clast was examined at the University of Arizona with an AML JEOL 840A/TN5502 scanning-electron-microscope (SEM) operated by the Materials Science and Engineering Department and with a Cambridge Instruments 120B SEM at the Department of Geosciences. The latter instrument was used to determine the modal composition of the clast over an area of ≈27 mm^2 that is free of obvious shock veins, using computer-aided discrimination of phases on backscattered-electron (BSE) images. Phase compositions were determined with a Cameca CAMEBAX SX-50 microprobe at the Department of Planetary Sciences, University of Arizona, using wavelength dispersive methods, an accelerating voltage of 15 kV, and a sample current of 5 or 10 nA. The lower sample current and a shorter analysis routine were used for feldspar and glasses to minimize beam volatility effects. Microprobe determinations of concentrations (expressed as oxides) have an estimated relative precision of ≤3–9% at the 0.5 wt% concentration level and an estimated detection limit of ≤0.01 wt% based on the formulas of Ziebold (1967). The modal and microprobe data were combined to determine the major-element bulk composition of the clast to an estimated precision of ≈1–4% for all oxides (≈1% for SiO_2), except for Na_2O and K_2O (≈11–14% precision), TiO_2 (≈30%) and P_2O_5 (≈75%).

INAA and Oxygen-Isotope Studies

Following SEM and microprobe work, a saw cut was made through Bovedy parallel to the original slab surface, creating a thin slab with the original exposed surface of the clast and a second, thicker slab. The latter was used to obtain splits of the clast and host for instrumental neutron activation analysis (INAA) and oxygen-isotope analysis. Two splits of host Bovedy (#1, 2.89 mg; and #2, 3.10 mg) and one split of the clast (2.59 mg) were analyzed for oxygen-isotopic composition at the University of Chicago. Host split #1 (3 fragments) was obtained from between 1 to 3.5 mm away from the clast-host contact, while split #2 (1 fragment) was obtained from adjacent to the clast. Two splits of the clast (#A, 2.39 mg; and #B, 2.94 mg) and one other split of host Bovedy (47.3 mg) were taken for INAA. Splits #A and #B each consisted of numerous fragments from various locations within the clast, while the INAA split of host Bovedy consisted of one fragment that contains a metallic shock vein. Three separate INAA irradiations were performed, including a 3-h irradiation at the TRIGA reactor at the University of Arizona, a 48-h irradiation at the University of Missouri, and (for Mg, Al, V, Mn) a 1-min Rabbit irradiation at the TRIGA reactor.

The composition of clast splits #A and #B determined by INAA are similar to one another and are in agreement with the major-element composition of the clast determined by modal reconstruction for all elements except Al, which has an unresolved discrepancy between the two techniques. The adopted Al concentration (1.43 ± 0.46 wt%) is the median value between the higher value determined by modal reconstruction and the lower value determined by INAA; the stated error encompasses both determinations (and their respective precisions). The split of host Bovedy obtained for INAA appears to be enriched in some siderophile elements compared to average ordinary chondrites, probably as a result of the metallic shock vein it contains.

DESCRIPTION OF THE CLAST

Form and Size

In both polished and rough surfaces the clast appears very light-colored (almost white) in ordinary light and has a sharp contact with the host. It is highly irregular in form (Fig. 1a). In backscattered-electron images, the margin of the clast appears to cut indiscriminately across normally zoned orthopyroxene grains, with no apparent change in the zoning pattern of the grains (Fig. 1b). This suggests that Bo-1 is a fragment of an igneous rock and that any chemical exchange between the host and clast was minimal. The clast is 4.5 x 7 mm across in the original slab surface, and sectioning suggests that it extends at least 4 mm in the third dimension, giving it a minimum volume of ≈126 mm^3.

Mineralogy, Texture and Phase Chemistry

The texture and mineralogy of Bo-1 are clearly that of an igneous rock and are described in detail below. The modal composition of the clast is given in Table 1. Orthopyroxene is by far the most abundant phase in the clast; a silica polymorph and feldspathic materials are also important constituents. Metal and sulfide are highly depleted in the clast compared to the host, and their low abundance is probably responsible for the clast's overall light-colored appearance. Representative microprobe analyses of phases in the clast are given in Table 2; the ranges of compositions in pyroxene and feldspar are shown in Fig. 2.

Orthopyroxene ($En_{92}Wo_{0.15}$ to $En_{74}Wo_{2.9}$; mean $En_{80}Wo_{1.5}$ based on 33 analyses) is characterized by equant or elongate grains, typically 100–300 μm across. Each grain is normally zoned with a Mg-rich core and a Fe,Ca-rich margin (Fig. 1b,c). Minor elements such as Ti, Al, Cr, Mn and Na increase from grain cores to margins (Table 2). These trends are consistent with igneous crystallization, in which elements that are moderately or strongly incompatible in orthopyroxene (Ti, Al, Na, Fe, Ca) are depleted in early-formed (grain core) orthopyroxene, unlike the compatible element Mg.

A silica mineral is composed of tabular grains up to 75 μm wide and 200 μm long, and more equant, blocky grains up to 200 μm across. This mineral contains an appreciable amount of FeO (0.1–0.5 wt%; Table 2), which implies that it is either tridymite or cristobalite (Deer *et al.*, 1966). The tabular shapes of the grains are more consistent with tridymite than with cristobalite, and therefore we will refer to the silica mineral as tridymite throughout the rest of the paper. The tridymite grains tend to occur in groups on the margins of large expanses of orthopyroxene (Fig. 1c,d).

Tridymite is cross-cut and rimmed by small amounts of clinopyroxene (augite and subequal pigeonite; Fig. 1d–f). Rims and veins are typically ≤5 μm wide. Discrete clinopyroxene rims are only present at the interface between tridymite and feldspathic regions, and not between tridymite and orthopyroxene. (In some

Table 1. Mode of Bo-1.

	vol%
orthopyroxene	83.8
tridymite	6.2
feldspar	5.8
sodic glass	3.1
pigeonite	1.0
chromite	0.2
augite	trace
Fe-Mg-glass	trace
metal	≤ 0.1
sulfide	≤ 0.1
ilmenite	0
phosphate	0
olivine	0

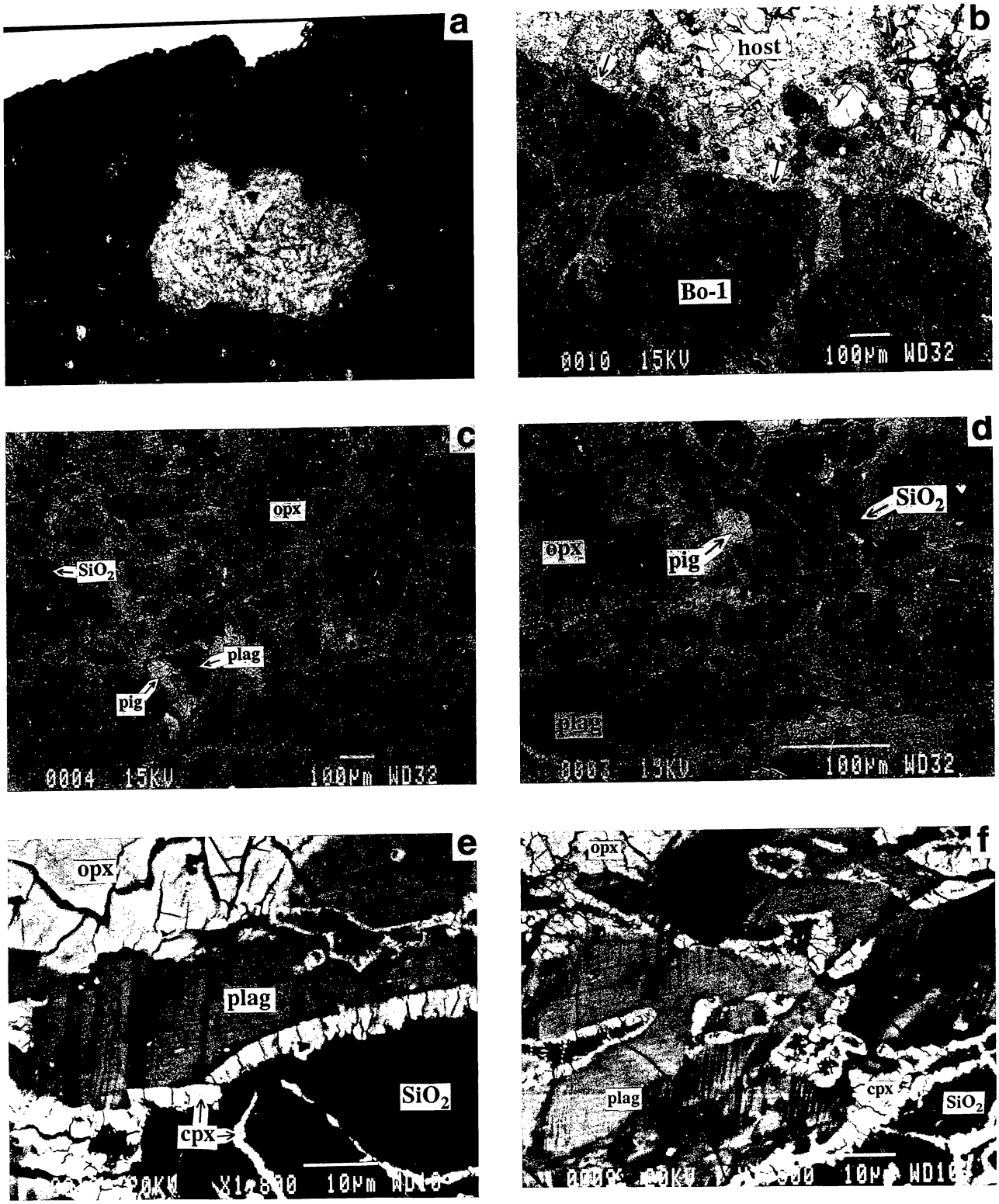

FIG. 1. Ordinary light (a) and BSE images (b–f) of the Bo-1 clast. **(a)** View of the light-colored clast (~ 4.5 x 7 mm across) as seen in a polished slab. The section edge is in the upper left corner. **(b)** Clast-host contact. The diffuse, mottled appearance of the clast is caused by normal igneous zoning in orthopyroxene, with Mg-rich grain cores appearing darker than Fe-rich grain margins. Arrows point to two locations where Mg-rich cores are in direct contact with the more Fe-rich host; these areas show no appreciable diffusional exchange between clast and host. **(c)** Overall texture of Bo-1 showing large expanses of normally zoned orthopyroxene (opx), equant and tabular grains of tridymite (SiO_2, black), small amounts of pigeonite (pig, light-grey), and anhedral regions of plagioclase and sodic glass (plag). **(d)** Higher magnification view of tridymite laths, subhedral pigeonite, and anhedral regions of plagioclase and sodic glass intergrowths. Tridymite is cross-cut and rimmed by clinopyroxene. **(e)** High-magnification view of lamellar intergrowth between plagioclase (plag, medium-grey) and a sodic, nephelinitic glass (dark-grey). Augite and pigeonite (cpx) form rims and veins in tridymite. **(f)** View of typical feldspathic region containing lamellar and diffuse intergrowths of plagioclase (medium-grey) and sodic glass (dark-grey).

instances, pigeonite intervenes between tridymite and orthopyroxene, but this pigeonite does not form a continuous rim around tridymite.) The composition of augite in rims and veins appears to vary greatly (Fig. 2), but this could be an artifact caused by the microprobe beam overlapping small-scale intergrowths of augite and pigeonite. The rims and veins are texturally continuous and chemically similar, suggesting that they both formed in the same way.

The rim and vein clinopyroxene is distinctive but represents a volumetrically insignificant part of the clast (<<1 vol%). Coarser (up to 100 μm across), more abundant (≈1 vol%) pigeonite is also present in the clast, and forms two textural types, anhedral and subhedral. Anhedral pigeonite is interstitial to large orthopyroxene grains and appears to extend the normal zoning pattern of the enclosed orthopyroxene grains to higher Wo and lower En contents (Table 2). This pigeonite contains rare, ill-defined patches of augite. Subhedral pigeonite is located adjacent to feldspathic regions and has well-formed crystal margins against these regions (Fig. 1d). This type of pigeonite appears to be enriched in Al, Ti and Cr compared to the anhedral pigeonite (Table 2). As with the anhedral pigeonite, the subhedral pigeonite is located on the margins of orthopyroxene grains (Fig. 1c,d).

Feldspathic regions (up to 200 μm across) are interstitial to orthopyroxene, tridymite and subhedral pigeonite, and consist mainly of bytownite-labradorite feldspar ($An_{77}Or_{0.26}$ to $An_{66}Or_{2.2}$) and a sodic glass (Fig. 2, Table 2). The feldspar and sodic glass typically form a fine-scale lamellar intergrowth (Fig. 1e,f). The lamellae are usually straight and locally parallel, although they are occasionally displaced along what appear to be microfaults that have also displaced adjacent clinopyroxene rim layers. In other areas, feldspar and sodic glass lack the lamellar texture and instead form larger, less regular intergrowths that have relatively rounded (and sometimes diffuse) contacts (Fig. 1f).

Table 2. Representative microprobe analyses of phases in the Bo-1 clast.

	1	2	3	4	5	6	7	8	9
wt%									
SiO_2	56.8	54.2	55.0	51.5	54.9	49.7	49.6	60.5	99.2
TiO_2	0.00	0.08	0.08	0.53	0.07	--	--	--	0.03
Al_2O_3	0.05	0.70	0.33	1.73	0.30	32.8	37.2	10.2	0.05
Cr_2O_3	0.12	0.75	0.29	0.88	0.32	--	--	--	0.04
FeO	8.83	15.0	12.4	17.4	7.35	0.18	0.19	5.08	0.36
MnO	0.14	0.42	0.37	0.42	0.38	--	--	--	0.00
NiO	0.08	0.07	0.00	0.06	0.00	--	--	--	0.00
MgO	34.4	27.7	27.2	18.7	20.3	0.04	0.02	10.8	0.10
CaO	0.11	1.27	4.99	8.84	16.60	15.14	4.23	7.16	0.06
Na_2O	0.01	0.09	0.12	0.24	0.23	2.71	7.53	4.79	0.03
K_2O	0.00	0.00	0.00	0.00	0.01	0.04	1.71	1.30	0.01
P_2O_5	0.00	0.01	0.00	0.06	0.00	--	--	--	0.02
total	100.5	100.3	100.9	100.3	100.4	100.6	100.6	99.8	99.9
mol%*									
En	87.2	74.8	72.0	53.7	55.8	--	--	--	--
Fs	12.6	23.3	18.5	28.0	11.4	--	--	--	--
Wo	0.2	1.9	9.5	18.3	32.8	--	--	--	--
An	--	--	--	--	--	75.3	(21.2)	(41.2)	--
Or	--	--	--	--	--	0.3	(10.2)	(8.9)	--
Ab	--	--	--	--	--	24.5	(68.6)	(49.9)	--

1: orthopyroxene grain core. **2:** orthopyroxene grain margin. **3:** anhedral pigeonite, interstitial to orthopyroxene. **4:** subhedral pigeonite. **5:** augite in clinopyroxene layer surrounding tridymite. **6:** bytownite feldspar. **7:** sodic glass. **8:** Fe,Mg-bearing glass. **9:** tridymite.
*** Symbols:** En = 100 Mg/(Mg+Fe+Ca), Fs = 100 Fe/(Mg+Fe+Ca), Wo = 100 Ca/(Mg+Fe+Ca), An = 100 Ca/(Ca+Na+K), Ab = 100 Na/(Ca+Na+K), Or = 100 K/(Ca+Na+K)

In terms of 8 oxygens per formula unit, the feldspar has the average composition $Na_{0.25}K_{0.01}Ca_{0.73}Fe^{3+}_{0.01}Al_{1.78}Si_{2.22}O_8$ (based on 13 analyses), while the sodic glass has the average composition $Na_{0.74}K_{0.10}Ca_{0.20}Fe^{3+}_{0.01}Al_{1.97}Si_{2.20}O_8$ (13 analyses). Although the sodic glass has a Ca/(Na + K) ratio that corresponds to oligoclase feldspar (Fig. 2; Ruzicka and Boynton, 1992a), it also has an Si/Al atom ratio (≈1.1) that is lower than would be expected for stoichiometric feldspar (≈2.6) based on the Ca/(Na + K) ratio. The sodic glass is, thus, deficient in Si (or enriched in Al) relative to stoichiometric oligoclase. In terms of normative minerals, the mean composition of the sodic glass can be expressed as 66.0 wt% plagioclase ($An_{30}Or_{16}$), 20.3% nepheline, 13.2% corundum, and 0.5% olivine (Fo_{18}). This composition is similar to a eutectic melt in the system forsterite-albite-nepheline (Schairer and Yoder, 1961), which has the approximate normative composition 74.1 wt% albite, 24.5% nepheline, and 1.4% forsterite. The presence of normative nepheline in the glass implies that it is silica-undersaturated, although the abundance of silica polymorph in the clast suggests that the clast is silica-oversaturated as a whole.

The similarity in composition between the sodic glass and a eutectic melt suggests that the sodic glass was a low-temperature melt. However, it is unclear why the sodic glass forms lamellar intergrowths with feldspar. Perhaps this texture formed by kinetic or nucleation effects during magmatic crystallization of feldspar, or by the devitrification of feldspar from a glass. Alternatively, it may have been produced by reaction of residual melt with feldspar along twin boundaries (Y. Ikeda, pers. comm.). The lamellae probably did not form by subsolidus alteration of feldspar, because there is

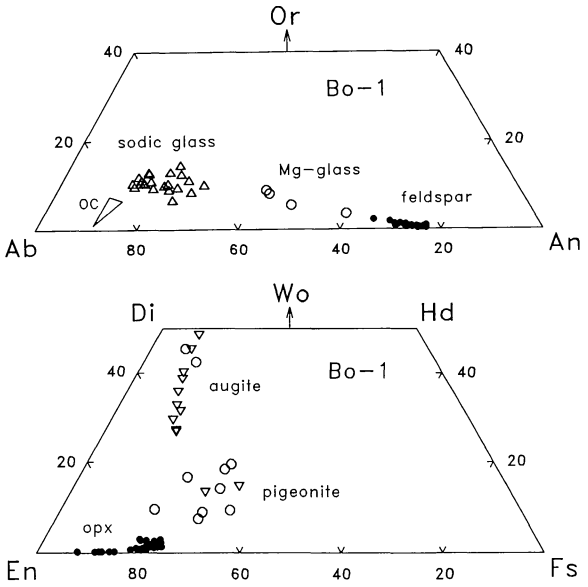

FIG. 2. Feldspar ternary (top) and pyroxene quadrilateral (bottom) diagrams showing the range of pyroxene, feldspar, and glass compositions in Bo-1. In the pyroxene diagram, open triangles represent clinopyroxene in rims and veins associated with tridymite, and open circles represent anhedral and subhedral clinopyroxene. OC = approximate range of feldspar composition in Type 6 ordinary chondrites. Symbols as in Table 2.

no reason to expect such alteration to produce a eutectic-like composition.

In any case, the apparent Si deficiency of the sodic glass and the presence of what appear to be reaction rims on tridymite suggest that some of the tridymite formed metastably, creating a slightly silica-undersaturated condition in the residual melt. The tridymite then reacted with the residual liquid to form the clinopyroxene rims in an attempt to re-establish local equilibrium, removing much of the Mg and Fe in the liquid to leave behind a liquid rich in Si, Al, Na, K and Ca. This residual liquid ultimately solidified into feldspar and the sodic glass.

Rare Fe,Mg-rich glass occurs in the mesostasis where rims on tridymite are locally absent. This glass has a Na, K and Ca content intermediate between the feldspar and sodic glass (Fig. 2, Table 2). The composition of this glass and the absence of nearby clinopyroxene rims suggest that it could represent the original residual liquid that failed to react with the adjacent tridymite to form rim-layer clinopyroxene. Alternatively, the Fe-Mg-rich glass could also have formed by localized shock melting of a mixture of feldspathic mesostasis, rim-layer clinopyroxene, and tridymite, perhaps in the same event that produced sulfide-rich shock veins in some places within the clast. No such obvious shock veins occur in the vicinity of Fe,Mg-rich glass, however, and the areas containing Fe-Mg-rich glass do not texturally resemble typical shock melt pockets in ordinary chondrites (Stöffler *et al.*, 1991).

Chromite is the most abundant opaque mineral in the clast and occurs as small inclusions within orthopyroxene. Occasionally, tiny (≈2-μm-diameter) metal inclusions are present in the geometric centers of some tridymite grains. These metal grains may have served as nucleation centers for the tridymite.

Crystallization and Cooling

The crystallization history of Bo-1 can be inferred from its texture. Tridymite and pigeonite (anhedral and subhedral) are located on the margins of orthopyroxene grains and thus largely crystallized after orthopyroxene, while feldspar crystallized even later because it is interstitial to these phases. Vein and rim clinopyroxene associated with tridymite must have formed after tridymite. Finally, the enclosure of chromite by orthopyroxene suggests that chromite crystallized before or during orthopyroxene. Thus, the crystallization sequence of Bo-1 may be summarized as follows: Mg-orthopyroxene ± chromite → Ca,Fe-orthopyroxene ± chromite → tridymite + pigeonite (anhedral and subhedral) → pigeonite/augite (vein and rim) + feldspar.

The igneous evolution of the clast can be evaluated by projecting its bulk composition (Table 3, col. 1) onto relevant ternary liquidus diagrams, the most useful being olivine-anorthite-quartz (Fig. 3), olivine-diopside-quartz, and forsterite-nepheline-quartz. Two crystallization models are shown in Fig. 3: (1) equilibrium crystallization, and (2) metastable crystallization, in which some disequilibrium (undercooling) is permitted. The composition of Bo-1 falls within the low-Ca pyroxene primary crystallization field (Fig. 3), and so a cooling melt of this composition is expected to first crystallize orthopyroxene. With continued cooling during equilibrium crystallization, a silica polymorph (either cristobalite or tridymite) will eventually join orthopyroxene, and this will in turn be followed by pigeonite and a silica polymorph, and finally by a diopsidic (or augitic) pyroxene, tridymite, and feldspar (Fig. 3). For metastable crystallization, the evolving liquids are not constrained to lie on cotectics or eutectics, and the liquid composition can overstep phase boundaries (Fig. 3). The tendency in this case will be to crystallize one phase at a time, namely orthopyroxene alone, then tridymite alone, and eventually plagioclase alone (Fig. 3).

Both of these predicted crystallization sequences generally resemble that inferred from the texture of the clast, reinforcing the conclusion that it crystallized from a melt. The high degree of crystallinity of Bo-1 (≈97 vol%) suggests an approach to equilibrium. On the other hand, there are indications of disequilibrium in the clast, including: (1) zoning in orthopyroxene; (2) no clear evidence for cotectic crystallization of orthopyroxene and tridymite; (3) the presence of tridymite and not quartz, the stable Si-polymorph at subsolidus temperatures (and low pressures); (4) the apparent (incomplete) reaction between tridymite and residual liquids; and (5) a small amount of glass. In particular, the presence of nephelinitic glass coexisting with silica polymorph and abundant orthopyroxene is significant and cannot be explained by equilibrium processes. Rather, this association implies that cooling occurred with sufficient rapidity so that one or more Si-rich phases, probably tridymite and possibly also orthopyroxene and feldspar, crystallized metastably. This could have driven the composition of the residual liquid away from a silica-oversaturated condition (where Si-polymorph is stable and olivine and nepheline are unstable) to a silica-undersaturated

Table 3. Chemical and normative composition (wt%) of Bo-1 compared to other rock types. mg# = Mg/(Mg+Fe) atomic; Si/Mg and Fe/Mn are weight ratios. All iron as FeO.

	1	2	3	4	5	6	7
SiO_2	57.5	46.2	47.8	60.8	54.4	53.1	54.5
TiO_2	0.04	0.17	0.20	--	0.12	0.08	0.29
Al_2O_3	2.72	2.91	3.50	3.09	3.32	0.57	5.22
Cr_2O_3	0.47	0.52	0.55	--	0.74	1.48	2.76
FeO	11.2	17.0	12.7	--	11.0	16.3	11.5
MnO	0.29	0.34	0.33	--	0.46	0.53	0.59
MgO	25.6	29.1	31.0	32.4	26.3	26.9	16.2
CaO	1.64	2.19	2.32	2.09	2.43	0.94	5.16
Na_2O	0.47	1.10	1.13	1.40	1.09	0.05	1.80
K_2O	0.07	0.17	0.16	0.20	0.21	0.0	0.20
P_2O_5	0.01	0.31	0.34	--	--	0.01	0.10
mg#	0.80	0.75	0.81	1.0	0.81	0.75	0.72
Si/Mg	1.74	1.23	1.20	1.46	1.61	1.53	2.60
Fe/Mn	38.8	50.7	38.6	--	23.9	30.9	19.5
Ol	0	54.5	48.1	0	11.3	5.1	0
Opx	83.3	25.6	31.1	77.5	66.6	88.2	53.2
Cpx	2.4	5.3	4.4	6.9	6.8	2.6	16.0
Plag	9.5	12.9	14.4	14.6	13.9	1.7	22.2
Chr	0.7	0.8	0.8	0	1.1	2.2	4.1
Ilm	0.1	0.3	0.4	0	0.2	0.2	0.6
Merr	0	0.7	0.7	0	--	0	0.2
Qz	4.1	0	0	1.1	0	0	3.7

1: Bo-1 clast. **2:** L-chondrite silicate (Mason, 1965). **3:** H-chondrite silicate (Mason, 1965). **4:** E-chondrite silicate (Mason, 1966). **5:** average radial-pyroxene chondrule in L3 stone Manych (Dodd, 1978). **6:** average diogenite (Dodd, 1981, p. 248). **7:** silicates in IIE iron Weekeroo Station (Olsen and Jarosewich, 1970). Ol = olivine, Opx = orthopyroxene, Cpx = clinopyroxene, Plag = feldspar, Chr = chromite, Ilm = ilmenite, Merr = merrillite, Qz = quartz.

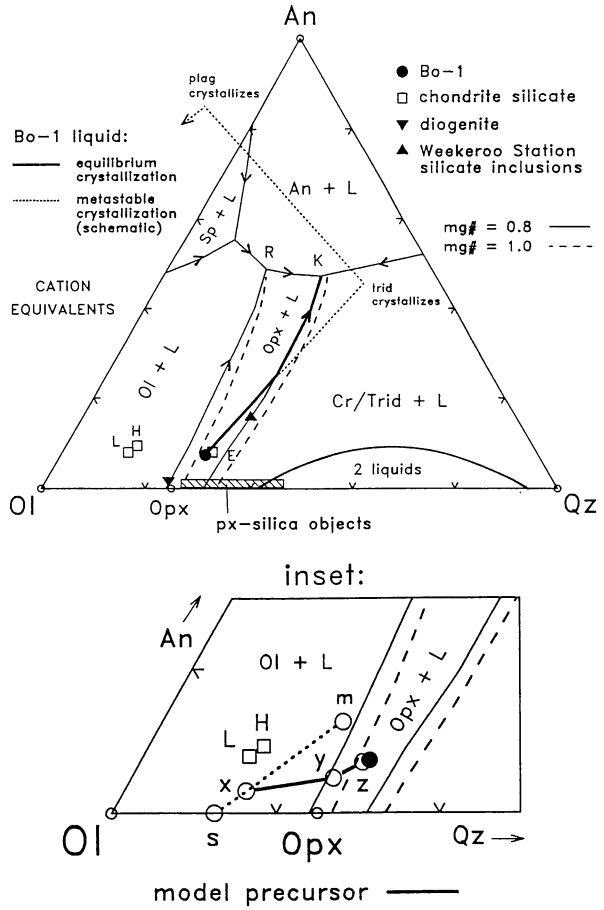

FIG. 3. Olivine-anorthite-quartz (Ol-An-Qz) pseudoternary liquidus diagram showing the projected compositions of Bo-1 and other objects (data from Table 3; Brigham *et al.*, 1986; Krot and Wasson, 1993), and liquid lines-of-descent for equilibrium and metastable crystallization of Bo-1. For equilibrium crystallization the Bo-1 melt will crystallize first low-Ca pyroxene (Opx) alone, then Opx + cristobalite (Cr) or Opx + tridymite (Trid), and finally Opx + Trid + An at eutectic point K. (In reality, clinopyroxene, not Opx, will be the last pyroxene to crystallize, and plagioclase will crystallize instead of pure anorthite.) For metastable crystallization, Opx, Trid, and plagioclase can crystallize singly in sequence, and Trid can become unstable in the residual liquid. The inset shows a model for generating the Bo-1 liquid from an ordinary chondrite-like precursor. Point x is the modelled bulk composition of a partial melt residue produced by the loss of 22% silicate partial melt at a (silicate melt)/(solid silicate + silicate melt) ratio of 0.25, and by the loss of 74% of the initial Fe in the form of metallic liquids and solids. In residue x, (trapped) peritectic melt m coexists with solid s, with the latter containing roughly equal proportions of Ol and Opx. A melt similar to Bo-1 in composition can be produced by continued partial or complete melting of x. Complete melting of residue x (mg# = 0.91) followed by the loss of 33% Ol by fractional crystallization forms a liquid with model composition y (mg# = 0.86), in which Opx can crystallize. Fractional crystallization of 27% Opx from liquid y produces a liquid with model composition z (mg# = 0.80), which is very similar to the Bo-1 melt. (Line y-z is a model trajectory that should be radial to Opx, but which is not, possibly owing to an error in one or more partition coefficients for Opx; such an error would not significantly affect our conclusions as to how Bo-1 formed.) With incomplete equilibrium melting of residue x, the composition of the liquid will move along the peritectic from m to y, and the solid will move along the Ol-Opx join from s to Ol. At y, the last Opx melts and the unmelted solid is pure Ol. Removal of Ol as an unmelted solid from liquid y, followed by fractional crystallization of Opx, can also produce a liquid chemically similar to Bo-1. Phase boundaries are shown for mg# = 0.8 and mg# = 1. The diagram was partly constructed by interpolation between experimental systems with mg# = 1 (Andersen, 1915) and mg# = 0.59 (Lipin, 1978); see Morse (1980).

condition (where Si-polymorph is unstable and nepheline and olivine are stable) (Fig. 3). It therefore appears that the Bo-1 melt cooled neither very slowly nor very rapidly but rather at some intermediate rate, fast enough to permit some disequilibrium but slow enough to allow nearly complete crystallization.

Oxygen-Isotopic Composition

The oxygen-isotopic composition of Bo-1 (Table 4) does not correspond to previously described meteorite types, but most closely resembles ordinary chondrites. The oxygen-isotopic composition of the clast is similar to chondrules in ordinary chondrites (Clayton *et al.*, 1991) and to silicate inclusions in IIE iron meteorites (Clayton *et al.*, 1983; Rubin *et al.*, 1986), but the clast always has higher $\delta^{18}O$ and mostly has higher $\delta^{17}O$ than these objects. The clast has higher $\Delta^{17}O$ ($=\delta^{17}O - 0.52\ \delta^{18}O$) than achondrites, which appears to rule out the possibility that Bo-1 is a xenolith from one of the commonly recognized achondrite groups.

An oxygen-isotope mass fractionation line through the clast passes almost exactly through the mean value for H-group chondrites, but the difference in $\delta^{18}O$ between Bo-1 and mean H-chondrites is rather large, close to 4‰ (Fig. 4). Part of this difference in $\delta^{18}O$ can be ascribed to the enrichment of silica polymorph and the absence of olivine in Bo-1 compared to H-group chondrites, as equilibrium partitioning results in a higher ratio of $^{18}O/^{16}O$ in quartz than in forsterite (Clayton and Kieffer, 1991), but the difference in $\delta^{18}O$ is too large for Bo-1 and H-group material to have been in isotopic equilibrium at the high temperatures appropriate for igneous processes. Thus, the clast probably did not form simply by the melting or igneous fractionation of H-group material. However, the overall similarity in oxygen-isotopic composition between Bo-1 and ordinary chondrites suggests that Bo-1 could have been derived from material similar to that from which ordinary chondrites formed.

Table 4. Oxygen isotopic composition of Bo-1 and two splits of host Bovedy (L3), compared with other silica-rich objects and ordinary chondrites. δ = per mil deviation from SMOW standard; $\Delta^{17}O = \delta^{17}O - 0.52\ \delta^{18}O$.

	$\delta^{18}O$	$\delta^{17}O$	$\Delta^{17}O$
Bo-1 clast	7.72	4.72	0.71
Bovedy host #1	6.79	4.27	0.74
Bovedy host #2	5.12	3.65	0.99
CRISPY[1]	8.80	6.50	1.93
tridymite[2]	5.71	3.70	0.73
CB1[3]	11.50	8.60	2.62
CB2[3]	11.48	8.56	2.59
H3-6[4] mean	3.91	2.83	0.71
s.d.	(0.62)	(0.16)	(0.09)
L3-6[4] mean	4.70	3.50	1.05
s.d.	(0.24)	(0.16)	(0.12)

1: cristobalite xenocryst in ALHA 76003 (L6), Olsen *et al.* (1981). **2:** tridymite inclusion in the Kendleton (L) breccia, Ehlmann *et al.* (1988). **3:** cristobalite-bearing clasts in Parnallee (L3), Bridges *et al.* (1993). **4:** whole-rock falls, Clayton et al. (1991). "s.d." refers to standard deviation from the mean.

The oxygen-isotopic composition of one split (#1) of host Bovedy lies on a mass-fractionation line consistent with H-chondrites, similar to the clast, while another split (#2) lies on a mass-fractionation line more consistent with L-chondrites (Fig. 4, Table 4). Although these results could be explained by the splits having experienced different degrees of oxygen-isotope exchange between Bo-1 and the surrounding L3 host, this is unlikely, as the split less similar to Bo-1 in oxygen-isotope composition was taken from closer to the clast. Another possibility is that host split #1 incorporated fragments from Bo-1, either by shock disruption or during sample preparation, but no such fragments were evident during microscopic examination. The discrepancy between the two host splits instead probably reflects the intrinsic oxygen-isotopic heterogeneity of type 3 ordinary chondrites (Clayton *et al.*, 1991) together with the small sizes of the samples (≈3 mg in this study compared to ≈100 mg used by Clayton *et al.*, 1991). The observation that host split #1 lies on nearly the same oxygen-isotope mass fractionation trend as Bo-1, H-group chondrites, and another previously studied Bovedy clast (Rubin *et al.*, 1981), could indicate that Bovedy contains a high proportion of H-chondrite-like material.

Like Bo-1, four other Si-rich objects in ordinary chondrites also have higher $\delta^{17}O$ and $\delta^{18}O$ than bulk ordinary chondrites (Table 4). These Si-rich objects do not all lie on the same mass fractionation trend (*i.e.*, they do not all have the same $\Delta^{17}O$ values), and so they cannot all be related by mass fractionation alone. They also do not lie on a single mixing line. This probably indicates that the Si-rich material in ordinary chondrites was derived from multiple sources.

Major-Element Composition

The major-element composition of Bo-1 is distinctly non-chondritic. The clast has a higher Si/Mg ratio and higher normative quartz content than chondrites, although its bulk mg# (= Mg/(Mg + Fe)) and Fe/Mn ratios are similar to H- and L-group silicate (Table 3). The major-element composition of Bo-1 is very similar to a glassy inclusion that was found in a different section of Bovedy (Hill, 1993), and also resembles: (a) radial-pyroxene and cryptocrystalline chondrules in ordinary chondrites, (b) pyroxene-silica objects in ordinary chondrites, (c) diogenites, and (d) silicate inclusions in the IIE iron meteorite Weekeroo Station (Fig. 3, Table 3). The Si/Mg ratio and the normative orthopyroxene and plagioclase contents of the clast are intermediate to that in diogenites and Weekeroo Station silicate (Fig. 3, Table 3).

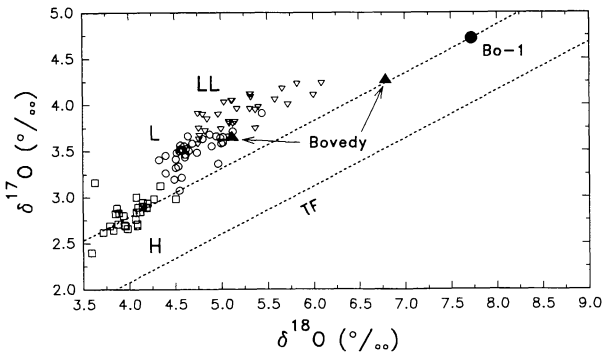

FIG. 4. Three-isotope oxygen plot showing the composition of Bo-1 and two splits of host Bovedy (this study, Table 4) and whole-rock H-, L-, and LL-group ordinary chondrites (Clayton *et al.*, 1991). Terrestrial mass-fractionation line is "TF"; a parallel mass-fractionation line also is shown passing through Bo-1.

Trace-Element Composition

Neutron-activation data for two splits of the clast are given in Table 5 and Fig. 5. In general, lithophile elements are modestly fractionated compared to CI or ordinary chondrites (Fig. 5a). The CI-normalized lithophile element abundances range from ≈2.5x CI (Si) to 0.1–0.4x CI (Hf, Ti, Cs, Br, Zn). Elements that are relatively incompatible in olivine and pyroxene are depleted in Bo-1 compared to CI and ordinary chondrites, while this is generally not the case for more compatible or major elements (Fig. 5a). These results suggest that Bo-1 could have formed in part from chondritic material that lost a silicate partial melt enriched in incompatible elements. In contrast to lithophile elements, siderophile and chalcophile elements are highly depleted in Bo-1 compared to both CI and ordinary chondrites (Fig. 5b). This is consistent with the low abundances of metal and sulfide in the clast. The CI-normalized abundances of siderophile elements and chalcophile element Se resemble a step function, with some

Table 5. Neutron activation results for two splits of the Bo-1 clast and for one split of host Bovedy. Values are in ppm except for Na, Mg, Al, K, Ca, Cr, Mn, Fe and Ni which are in wt%, and Ru, Re, Os, Ir, Au, and Th which are in ppb.

	Bo-1 clast # A	pre-cision (%)	Bo-1 clast # B	pre-cision (%)	Bovedy host	pre-cision (%)
Na	0.2826	0.3	0.331	0.4	0.642	0.6
Mg	--	--	23.	25.2	16.	8.5
Al	0.94	5.4	1.10	4.3	1.10	1.6
K	0.041	5.4	0.051	4.7	0.082	2.2
Ca	1.24	4.1	1.66	4.2	0.7	25.6
Sc	4.14	0.7	4.23	0.8	7.20	0.7
V	--	--	80.	19.0	65.	6.2
Cr	0.309	0.9	0.328	0.9	0.322	0.4
Mn	0.27	11.5	0.25	11.1	0.242	2.4
Fe	7.89	0.6	8.24	0.5	35.7	0.3
Co	8.68	0.6	7.65	0.7	1906.	0.3
Ni	0.0115	1.7	0.0027	5.7	2.04	0.8
Zn	40.2	1.4	44.0	1.1	76.	8.6
Ga	--	--	--	--	5.8	6.9
Se	--	--	--	--	7.	20.0
Br	1.33	3.3	1.63	4.1	--	--
Rb	1.2	22.4	1.4	9.7	--	--
Sr	--	--	5.	26.4	--	--
Ru	140.	9.6	70.	17.9	--	--
Cs	0.08	13.3	0.106	9.0	--	--
La	0.154	3.4	0.191	4.6	0.36	11.3
Ce	0.52	7.9	0.55	6.9	--	--
Nd	0.26	23.4	0.38	14.7	--	--
Sm	0.108	2.0	0.131	2.0	0.171	1.6
Eu	0.044	3.4	0.054	2.1	--	--
Tb	0.025	11.2	0.025	10.0	--	--
Ho	--	--	--	--	0.10	17.4
Yb	0.141	2.8	0.157	3.2	--	--
Lu	0.020	5.1	0.022	3.2	--	--
Hf	0.05	20.4	0.061	12.0	--	--
Re	9.	28.1	--	--	--	--
Os	217.	2.6	90.	6.0	750.	10.7
Ir	118.8	0.3	5.87	0.8	543.	1.1
Au	1.8	8.8	--	--	339.	0.7
Th	0.17	26.2	--	--	--	--

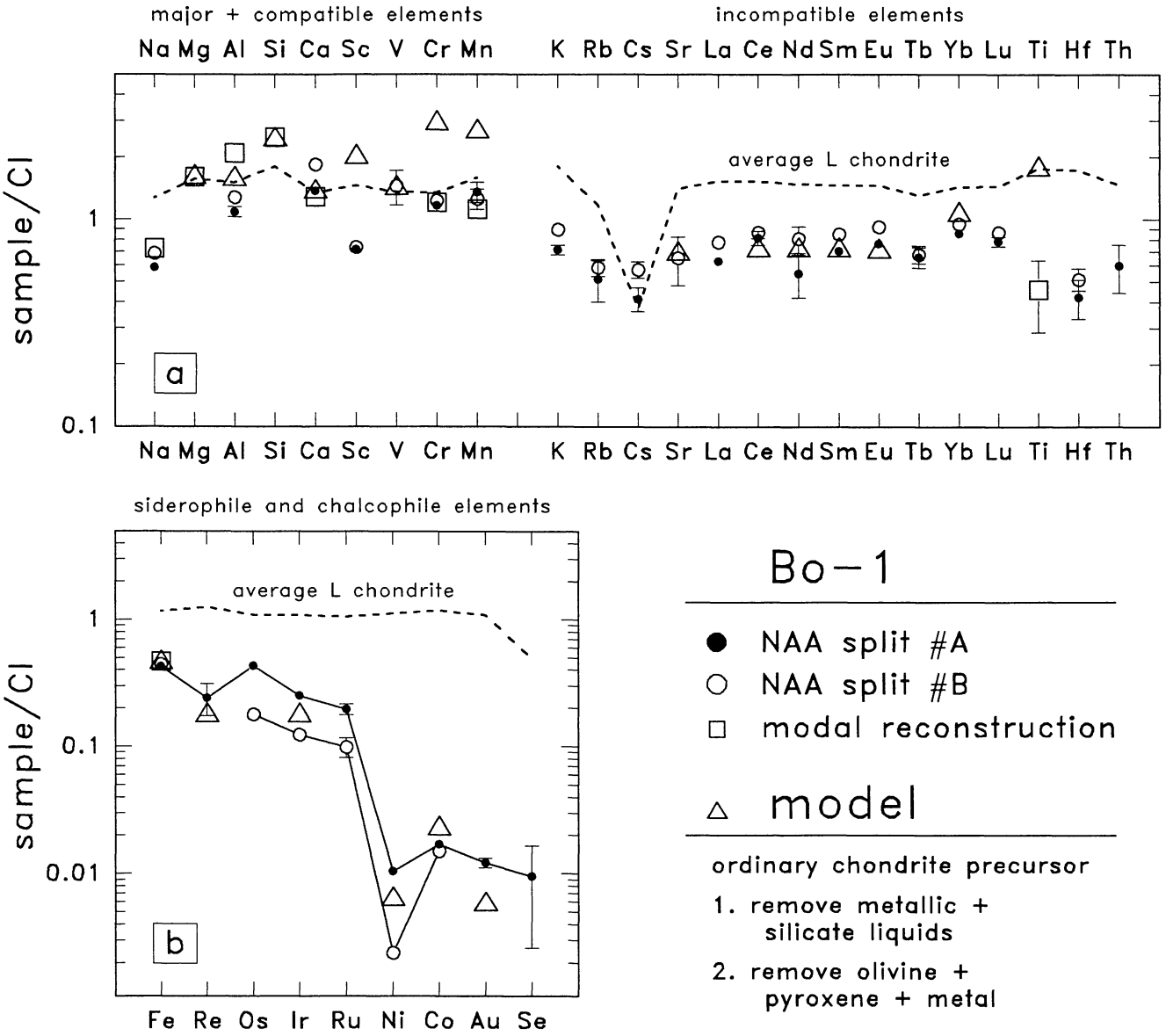

FIG. 5. The CI-normalized elemental abundances of Bo-1 compared to the predictions of a model assuming igneous fractionation of an L-chondrite precursor. Similar model results are obtained by assuming an H-chondrite precursor. Predominantly lithophile elements are shown in **(a)** and predominantly siderophile and chalcophile elements are shown in **(b)**. The model involves the following: (1) Loss of all metallic melt and most silicate melt during equilibrium partial melting. The (metallic melt)/(solid metal + metallic melt) fraction is 0.90, the (silicate melt)/(solid silicate + silicate melt) fraction is 0.25, and 22% silicate melt is removed from the silicate system. (2) Loss of 80% of the remaining metal, all of the olivine, and some low-Ca pyroxene at a higher degree of melting. The specific model shown involves complete melting, followed by the removal from this melt of 33% olivine by fractional crystallization to form a peritectic melt, followed by the removal from the peritectic melt of 27% low-Ca pyroxene by fractional crystallization to produce melt z (see Fig. 3). Seventy-four wt% of the initial Fe in the precursor is lost from the original precursor in metallic phases. Sources of partitioning data: Re, Ir, Ni, Co and Au–Jones and Drake (1986); other elements–Table 6. Sources of L-chondrite data: major elements–Mason (1965); Sr and Re–Mason (1971); rare-earth-elements–Masuda *et al.* (1973); other trace elements–Kallemeyn *et al.* (1989).

siderophile elements (Fe, Re, Ru, Ir, Os) being depleted to ≈0.1–0.4x CI, and other elements (Ni, Co, Au, Se) being depleted to ≈0.002–0.02x CI (Fig. 5b). The latter four elements should partition strongly into a S-bearing metallic melt, and thus their depletion relative to other siderophile elements is evidence that Bo-1 lost some metal and sulfide in the form of metallic melt.

ORIGIN OF THE BO-1 LIQUID

Hypotheses for Forming Silica-rich Material

Many different hypotheses have been advanced to explain the origin of Si-rich material in meteorites. Most of these fail to adequately explain the origin of the Bo-1 liquid, as we show below before proceeding to our preferred interpretation.

Collision-induced melt phase separation, in which the residual melt of chondrules is separated from coexisting crystals by impact (Brigham *et al.*, 1986; Nakamura *et al.*, 1990), could not produce the composition of Bo-1 because such liquids are rich in Al and normative feldspar. The removal of a high-temperature condensate, which would leave behind material depleted in refractory elements and enriched in non-refractory elements such as Si (Brigham *et al.*, 1986; Nakamura *et al.*, 1990), does not explain the enrichment of Si, Al, and Ca compared to elements of similar volatility in Bo-1.

Redox and metal loss processes (Brigham *et al.*, 1986) are by themselves incapable of changing the Si/Mg ratio and, thus, cannot explain the high Si/Mg ratio of Bo-1 unless a non-chondritic precursor is assumed.

The similarity in composition between Bo-1 and radial-pyroxene and cryptocrystalline chondrules raises the possibility that Bo-1 may have formed from a melt involving either precursors or processes (or both) similar to that which formed these chondrules. As it is unclear how the distinctive composition of these chondrules arose, the similarity in composition between them and the Bovedy clast is unfortunately more tantalizing than instructive. However, the clast differs from chondrules in some important ways, including: (1) the large melt volume, with >126 mm^3 for the clast compared to 0.01–0.4 mm^3 for typical (0.3–0.9-mm-diameter; Grossman *et al.*, 1988) chondrules; (2) the high degree of crystallinity, with the low abundance of glass in Bo-1 suggesting that the melt cooled more slowly than most chondrule melts (*e.g.*, Grossman *et al.*, 1988); and (3) the irregular and apparently broken margin of Bo-1, suggesting that it formed by the brecciation of an even larger rock mass, and not necessarily as an independent, suspended object, as is true for many (or all) chondrules (*e.g.*, Grossman *et al.*, 1988). These differences lead us to conclude that Bo-1 did not form in a typical chondrule-forming event.

The separation of a Si-rich immiscible liquid can produce highly siliceous material, but cannot easily explain material with an intermediate Si content similar to Bo-1. This is illustrated by the location of the two-liquid immiscibility field in the olivine-anorthite-quartz pseudoternary system, which has limits that do not closely approach the Bo-1 composition (Fig. 3).

Given the large size of the clast and its overall chemical similarity to some igneously-formed pyroxenites like diogenites, it seems most likely that the clast formed by the igneous fractionation of a melt on an initially chondritic parent body. Such melts are usually attributed to internal heating processes associated with radionuclides or electromagnetic induction, particularly in the case of the HED parent body (*e.g.*, Hewins and Newsom, 1988). Alternatively, bulk chondritic melts could have been produced by impact processes, because the average collisional velocity among asteroids is large enough to produce a significant volume of impact melt (Stöffler *et al.*, 1991). These processes produced several ordinary chondrite impact melt breccias (*e.g.*, Dodd and Jarosewich, 1976; Kring, 1993), and fragments of impact melts in several ordinary chondrites (Fodor and Keil, 1976a,b; Keil *et al.*, 1980; Rubin *et al.*, 1981). We will return to this discussion after we present our detailed model for forming the Bo-1 liquid.

Major- and Trace-Element Modelling: Igneous Fractionation

The igneous texture and mineralogy of Bo-1 indicate that it crystallized from a siliceous melt, and the similarity in oxygen-isotopic composition between Bo-1 and ordinary chondrites and the presence of the clast in an ordinary chondrite host suggest that the melt could have been derived from an ordinary chondrite-like parent. Assuming an ordinary chondrite-like precursor, the trace- and major-element composition of the Bo-1 liquid can be successfully modelled as an igneous differentiate, if the precursor lost both its lowest-melting-temperature material (metallic and silicate melt) and its highest-melting-temperature material (olivine and metal). Roughly 70% of the original mass of the precursor would have been fractionated from the source region of the clast. During differentiation, metallic and silicate liquids appear to have been lost at an early stage of partial melting, and olivine and low-Ca pyroxene appear to have been lost at a later stage of partial or complete melting.

In our model, trace siderophile elements (Re, Ir, Ni, Co and Au) were assumed to have partitioned exclusively into metallic phases (solid and liquid metal) and other elements, except Fe, were assumed to have partitioned exclusively into silicate phases (silicate melt, olivine, low-Ca pyroxene, and feldspar). The partitioning of Fe in silicate and metallic phases will depend on f_{O_2}, and as this is not well constrained, the amount of Fe that could partition into metallic phases relative to silicate phases was treated as a free parameter. Mineral/melt partition coefficients for trace siderophiles were taken from Jones and Drake (1986), and partition coefficients for other elements were taken from the variety of sources given in Table 6.

Figure 3 illustrates how the major-element composition of Bo-1 can be obtained from an ordinary chondrite-like precursor through igneous differentiation, and Fig. 5 compares the major- and trace-element abundances in Bo-1 with those predicted by our model. The fractionation steps involved in the model are discussed in more detail below.

Metal and Sulfide Loss–Low abundances of metal and sulfide, low Fe/Mn, and low abundances of siderophile and chalcophile elements (Fe, Re, Os, Ir, Ru, Ni, Co, Au, Se) in Bo-1 compared to whole-rock ordinary and CI chondrites imply that metal and sulfide were removed from the precursor. The Fe/Mn ratio is sensitive to metal loss but to first order is unaffected by partial melting or fractional crystallization. The Fe/Mn ratio of Bo-1 is similar to the *silicate fraction* of H-chondrites (Table 3), which implies that Bo-1 could have formed from an H-chondrite that lost all of its preexisting metal. On the other hand, the lower Fe/Mn ratio in Bo-1 compared to L-chondrite silicate (Table 3) implies that Bo-1 could have formed from a L-chondrite precursor only if this precursor was reduced, with some of the original FeO converted to metallic Fe that was subsequently removed.

To obtain the best agreement for the largest number of modelled elements (Fig. 5), Bo-1 would have formed from an ordinary chondrite-like precursor that lost ≈65–75 wt% of its initial Fe in the form of metallic phases during melting. For comparison, the average (metallic Fe)/(total Fe) ratio is ≈0.29 in L-chondrites and ≈0.60 in H-chondrites (Mason, 1965). These results suggest that even with an H-chondrite precursor, some reduction during melting would have had to occur. Alternatively, the precursor could have been slightly more reduced than an average H-chondrite.

Trace-element abundances of siderophiles in Bo-1 are best explained by the removal of both a S-bearing metallic partial melt and by the subsequent removal of the residual (solid) metal. Sulfur-bearing metallic liquids need to be removed in order to account for the very low abundances of Ni, Co, Au, and Se (Fig. 5b), while additional (solid) metal needs to be removed to account for the overall depletion level of other siderophile elements (Re, Ir, Ru, Os) (Fig. 5b). Mass balance constrains the relative proportion of metallic liquid and solid that would have to be removed, assuming equilibrium between solid and S-bearing liquid metal. For an ordinary chondrite precursor, the optimal model (Fig. 5b) involves: (1) loss of an equilibrium partial melt at a (liquid metal)/(solid metal + liquid metal) fraction of 0.90–0.95, and (2) subsequent loss of 77–80% of the remaining solid metal. Steps (1) and (2) remove all but 2–4% of the initial metal + sulfide

complement, leaving only ≈0.25 wt% metal + sulfide in the system, which agrees with the observed abundance of metal and sulfide in the clast (Table 1).

The temperature at which metallic liquid was lost can be estimated from the Fe-S phase diagram (Hansen and Anderko, 1958) by knowing the Fe/S ratio in H- and L-chondrites and the fraction of metal that was melted at the time of metallic melt loss. This temperature is 1375 ± 10 °C for an H-chondrite precursor and 1295 ± 10 °C for an L-chondrite precursor, or roughly 1335 ± 50 °C.

Loss of Silicate Partial Melt–Incompatible lithophile elements (such as rare-earth-elements) are depleted in Bo-1 compared to L- and H-chondrites, with abundances of ≈0.8x CI in the clast and ≈1.3–1.6x CI in ordinary chondrites (Fig. 5a). Forming Bo-1 from either an H- or L-chondrite precursor requires the removal of a partial melt enriched in these incompatible elements. However, the relatively unfractionated abundances of incompatible lithophile elements in Bo-1 (Fig. 5a) indicate that some of the melt remained trapped in the solid residuum. Figure 6 shows that nearly uniform depletions of rare-earth-elements can be obtained in a residuum if some melt is removed, and some is retained, in the residuum. The lower the degree of partial melting, the proportionately less melt one must trap to obtain a relatively uniform depletion (Fig. 6). Incomplete removal of melt might be expected on low-gravity objects, where melt buoyancy could not easily overcome surface-tension or frictional forces in a crystal + liquid mixture, especially if (as was probably the case) the silicate liquid and solids had similar densities.

Table 6. Mineral/melt partition coefficients for olivine (ol), low-Ca pyroxene (opx) and plagioclase (plag) used in this study.

	ol	opx	plag	references [ol,opx,plag]
Mg	1.7-4.7	2.2-2.3	0.04	[1, 1, 2]
Fe	0.5-1.3	0.52-0.56	0.04	[1, 1, 2]
Cr	0.4-1.0	0.60-4.8	0.08	[1, 1, 2]
Si	0.8	1.08	1.02	[1, 1, 2]
Al	0.003	0.03-0.40	1.63	[1, 1, 2]
Ca	0.03	0.04-0.16	1.95	[1, 1, 2]
Sr	0.003	0.002	1.4	[3, 4, 1]
Sc	0.265	1.4	0.007	[3, 3, 5]
Mn	0.4-1.3	0.7	0.05	[6, 7, 7]
Ti	0.024	0.01-0.38	0.05	[7, 1, 2]
V	0.04	2.8	0.05	[7, 7, 8]
Ce	0.00007	0.0017	0.030	[9, 4, 5]
Nd	0.00007	0.0058	0.017	[9, 4, 5]
Sm	0.00058	0.011	0.017	[9, 4, 5]
Eu	0.0008	0.0068	1.1	[9, 4, 1]
Gd	0.0010	0.021	0.003	[9, 4, 5]
Yb	0.0194	0.087	0.007	[9, 4, 5]

[1] Weill and McKay (1975); "FMG" composition only for Cr,Si,Al,Ca; low f_{O_2} case for Eu. Range for Mg, Fe, Cr, Al, Ca and Ti caused by temperature dependence. **[2]** Villemant et al. (1981). **[3]** McKay and Weill (1977). **[4]** McKay et al. (1991), pigeonite Wo5. **[5]** Phinney and Morrison (1990); Nd and Gd interpolated. **[6]** Watson (1977), Si/O ≈ 0.27. Range caused by temperature dependence. **[7]** Irving (1977). **[8]** assumed to be the same as for Ti. **[9]** McKay (1986); Ce assumed to be the same as for Nd, Eu interpolated.

Removal of silicate melt must have occurred at high degrees (≥12–15%) of silicate partial melting to ensure that essentially all plagioclase in the source region was melted; otherwise a positive Eu anomaly would be preserved in the crystal-liquid residuum (Fig. 6). Similarly, extraction of silicate melt at low degrees of melting (≤15%) results in residues that are too rich in Ca, Al, and Yb relative to Mg and Si to permit the Bo-1 composition to be ultimately attained. Extraction of melt at very high degrees of silicate melting (≥65%), on the other hand, results in residues that are too depleted in Ca, Al, Si, and V relative to Mg to permit the Bo-1 composition to be attained. Good agreement between modelled and observed abundances for the key elements Mg, Si, Ca, Al, and V is obtained when silicate melt loss occurs at a (silicate melt)/(solid silicate + silicate melt) ratio of 0.2–0.3, with 25% silicate partial melting giving optimal results.

With 20–30% silicate partial melting, the unmelted grains consist of both olivine and low-Ca pyroxene, and model results suggest that melt was trapped in the interstices of the grains in the proportion (trapped melt)/(crystals + trapped melt) ≈ 0.04–0.05. The trapped melt is feldspathic, and therefore the bulk composition of the residue (x in Fig. 3) lies above the olivine-pyroxene join, albeit at a much lower normative feldspar content than bulk ordinary chondrites (Fig. 3).

Loss of Olivine and Low-Ca Pyroxene–The high Si/Mg ratio of the clast is best explained by the removal of magnesian olivine and low-Ca pyroxene from the melt out of which Bo-1 ultimately crystallized. As explained below, olivine and low-Ca pyroxene were apparently removed from the Bo-1 source region after silicate and metallic melt were removed, and at a temperature higher than that at which metallic and silicate melt were removed. This implies that olivine and pyroxene were fractionated either after continued melting of the earlier-produced partial melt residue, or in a later, higher-temperature remelting episode.

Complete melting of the earlier-produced residue (composition x in Fig. 3) results in a liquid that will first crystallize olivine upon cooling. Fractional crystallization of ≈30–40% olivine from this melt drives the composition of the melt to point y in Fig. 3, at

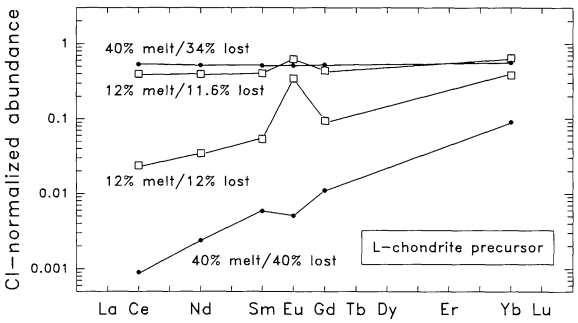

FIG. 6. Rare-earth-element (REE) diagram illustrating the effect of complete and incomplete removal of silicate liquids on residues produced during partial melting of an L-chondrite precursor. Models assume equilibrium melting and mass balance. Two silicate melt fractions (12% and 40%) are shown. Complete removal of the melt (12% melt/12% lost and 40% melt/40% lost) results in residues that are strongly depleted in REE (especially light REE) and other highly incompatible elements. However, incomplete removal of the melt (12% melt/11.6% lost and 40% melt/34% lost) results in residues that are less depleted and that are relatively unfractionated. Residues show positive Eu anomalies at low degrees of partial melting (<12–15%) because some plagioclase remains unmelted. Bo-1 could have formed from a partial melt residue of an ordinary chondrite that underwent incomplete melt removal at high degrees (≥12–15%) of partial melting. Calculations assume the partition coefficients given in Table 6 and the same L-chondrite data source as for Fig. 5.

which moment any remaining olivine begins to disappear by reaction with the melt and low-Ca pyroxene begins to crystallize. Fractional crystallization of ≈25–27% low-Ca pyroxene from melt y then drives the composition of the liquid to point z, which is very similar to the Bo-1 melt (Figs. 3, 5), and out of which Bo-1 could have crystallized.

A melt similar to Bo-1 in composition can also be obtained by continued, but less than complete, equilibrium melting of the earlier-formed partial melt residue, so long as heating is sufficient to melt all of the pyroxene in the residue. With continued heating of the initial olivine + pyroxene + trapped melt residue, pyroxene is preferentially melted, and the "trapped melt" grows in volume and becomes richer in normative pyroxene, while the solid becomes richer in normative olivine (the melt composition will change from m to y and the solid composition will change from s to Ol in Fig. 3). When the last of the pyroxene melts, the melt attains composition y (Fig. 3). Removal of the unmelted olivine from melt y, followed by fractional crystallization of low-Ca pyroxene from this melt, drives the liquid along essentially the same composition trajectory as before to the Bo-1 model liquid (Fig. 3).

The two scenarios described above for olivine fractionation yield very similar results, but represent extremes in (1) the temperature at which olivine is fractionated and in (2) the maximum heating temperature. Removal of all olivine by fractional crystallization requires complete melting, while removal of all olivine as an unmelted residue requires heating sufficient only to completely melt all of the pyroxene and to produce melt composition y in Fig. 3. Based on the olivine-anorthite-quartz phase diagram, composition y melts at ≈1480 °C, and this corresponds to the minimum heating temperature and the minimum temperature at which olivine was fractionated in the precursor. This temperature estimate is very approximate, because the phase diagram on which it is based necessarily represents an oversimplified system.

Olivine may also have been fractionated through a combination of fractional crystallization and the separation of an unmelted residue. This could have occurred if the heating temperature was sufficiently high to melt all of the pyroxene but not all of the olivine in the residue. After all of the pyroxene is melted, continued melting enriches the melt in normative olivine (with the melt composition changing from y to x in Fig. 3). As soon as the system begins to cool at any stage of such partial melting, the unmelted olivine can separate from the melt (by compaction and settling of the crystals), and olivine can crystallize and separate from the melt (by fractional crystallization); both processes will drive the composition of the remaining liquid to composition y at the peritectic. Fractional crystallization of low-Ca pyroxene from melt y can then produce the Bo-1 model liquid the same way as before.

Whichever mechanism was responsible for olivine fractionation, it appears that some low-Ca pyroxene separated from the Bo-1 melt precursor by fractional crystallization, after olivine was removed. This is suggested both by the model results and by the projection of the Bo-1 composition to well *within* the low-Ca pyroxene field (Fig. 3), although the latter could also be explained by metastable crystallization of olivine in the low-Ca pyroxene field. Fractional crystallization of low-Ca pyroxene in the immediate liquid precursor to Bo-1 is also consistent with the presence of normally zoned orthopyroxene in the clast.

Evaluation of Model Results

The elemental abundances predicted by the above model are very similar to the measured (adopted) concentrations in Bo-1 for many elements, to within 6% for Mg, Si, Fe, Al, Ca, V, Sr, Ce, Nd, Sm, Eu, and Yb, and mainly to within the variations between splits #A and #B for Re, Ir, Ni, Co, and Au (Fig. 5). This agreement for so many elements of differing geochemical behavior suggests that the main fractionation steps involved in the model are valid. The matches for Sc, Cr, Mn, and Ti are not satisfactory, however (Fig. 5). This could indicate that the partition coefficients assumed for these elements (Table 5) are not appropriate. Alternatively, these elements may have been strongly partitioned into fractionating phases of relatively low abundance, such as high-Ca pyroxene, chromite, and ilmenite. These "minor" phases are not considered in the model, and all of them are depleted in Bo-1 relative to ordinary chondrites (*cf.* Table 3). If these phases were partially removed from the Bo-1 source region during differentiation, then it would help explain why the observed abundances of Sc, Mn, Cr, and Ti are lower than predicted (Fig. 5a).

DISCUSSION

Heating Mechanism and Provenance of Bo-1

The Bo-1 melt could have formed from an ordinary chondrite-like precursor after various, non-isothermal igneous fractionation events (see above). Silicate and metallic liquids could have been removed at about the same time during an early stage of partial melting at relatively low temperatures, while olivine and low-Ca pyroxene could have been removed in a later stage of melting at a higher temperature. Such igneous differentiation can be explained by a single melting episode with a gradual increase in temperature up to the moment of olivine removal, or by two melting episodes, with the second involving higher temperatures than the first.

In a model with one melting episode, the precursor would have experienced a sustained period of heating of sufficient duration to allow metallic and silicate liquids to separate as temperature was increasing. After a continued rise in temperature, the system would begin to cool, and first olivine and then low-Ca pyroxene would fractionate from the melt, with the melt crystallizing to form Bo-1. In a model with two melting episodes, metallic and silicate liquid would have separated in the first episode of melting, and olivine and low-Ca pyroxene would have separated in a second episode of melting.

Melting may have occurred as a result of heating by radionuclides, electromagnetic induction, or hypervelocity impact. The first two mechanisms involve relatively long time scales for heating and cooling, whereas the latter involves essentially instantaneous heating followed by either a short or long time period of cooling (depending on circumstances).

Heating by hypervelocity impact is inconsistent with one melting episode for the Bo-1 precursor, because the temperature increase for this process occurs too rapidly to allow metallic and silicate liquid to separate before olivine and pyroxene are fractionated. Thus, if the Bo-1 precursor was melted once, then heating by radionuclides or electromagnetic induction are most likely to have been responsible for the melting. In the case of two melting events, radioactive decay and electromagnetic induction are again viable heat sources. Impact melting may be viable for the first melting event, but it is unlikely for the second, as special

circumstances would be required. Assuming that an initial melting episode produced a residue depleted in metallic and silicate partial melt, a later impact-melting episode would have had to have been both intense (to significantly melt the residue) and limited in spatial extent (to prevent mixing of the previously differentiated target). This combination of circumstances seems implausible. Consequently, the Bo-1 precursor was either melted once through radioactive decay or electromagnetic induction, or it was melted twice, with these same processes being responsible for at least the second episode of melting.

The igneous differentiation events we infer for the Bo-1 precursor must have occurred on a parent object with a significant gravitational field, which would allow phases of differing density to separate from one another. During the inferred early stage of partial melting, low-density silicate melt would tend to rise and high-density metallic melt would tend to sink, forming an upper feldspathic unit and a lower metallic unit. During the inferred later stage of melting, metal and olivine would sink relative to the remaining lower-density pyroxenitic melt, with an olivine-rich unit forming above the lowermost metal-rich unit, and the pyroxenitic melt crystallizing below the earlier-produced, feldspathic upper unit. According to our model results, Bo-1 could have crystallized from the pyroxenitic melt. The clast may therefore be a sample from the intermediate-to-upper level of a chemically and mineralogically stratified magma body.

Extensive melting of the precursor by either electromagnetic induction or radioactive decay could not have occurred without obliterating chondritic textures throughout a large fraction of the parent body. If either of these heating mechanisms were involved in the formation of Bo-1, as seems likely, then the clast probably did not originate on the Bovedy parent body, and is instead a sample of a different, extensively differentiated asteroid or planetesimal. Fragments of this differentiated asteroid could have been transported to the Bovedy parent body by a later impact.

The stratified magma body inferred for the Bo-1 source region could correspond to an individual magma chamber on a partly-to-completely differentiated asteroid, or it could correspond to an entire asteroid that had a core-mantle-crust structure. The pyroxenitic composition of Bo-1 is similar to that expected for the upper mantle of a differentiated ordinary chondrite asteroid (Taylor *et al.*, 1993), but the clast did not crystallize as slowly as might be expected for a deep-seated mantle rock. It therefore seems more likely that Bo-1 was derived from an individual, near-surface magma chamber on a differentiated asteroid than from deep within such an asteroid.

Other Silica-rich Objects in Ordinary Chondrites

Despite the diverse nature of other silica-rich objects in ordinary and carbonaceous chondrites and the equally diverse theories that have been proposed to account for them (see "Introduction"), some of these objects may have also originated in fractionating magmas.

Among other Si-rich objects, the case for magmatic differentiation seems strongest for those that contain K-feldspar. These objects contain variable amounts of orthopyroxene, clinopyroxene, K-feldspar, tridymite, ilmenite, and phosphate; zircon has also been found in some of them (Bischoff *et al.*, 1993; Wlotzka *et al.*, 1983). They are clastic, relatively crystalline, and sometimes show textures suggestive of slow cooling. These clasts have been described as alkali granitoids (Bischoff *et al.*, 1993) and could have formed as cumulates by fractional crystallization at or near the eutectic (point K in Fig. 3).

Pyroxene-silica objects are the most numerous Si-rich objects in ordinary chondrites, have either droplet or clastic forms, and are composed almost entirely of pyroxene and a silica mineral (Brigham *et al.*, 1986; Bridges *et al.*, 1993; Krot and Wasson, 1993). The compositions of these objects plot near the olivine-quartz join on the olivine-anorthite-quartz ternary diagram, straddling but not limited to the orthopyroxene-quartz eutectic (Fig. 3). These compositions can be produced as pyroxene-silica cumulates by cotectic fractional crystallization of pyroxene and a silica mineral from any melt that is dominated by normative pyroxene and quartz and that is relatively low in normative feldspar (such as a melt of Bo-1 or of Weekeroo Station silicate; Fig. 3). Pyroxene-silica cumulates produced in magnesian systems will generally contain more silica polymorph than in ferrous systems, which appears to agree with trends observed for pyroxene-silica objects (Krot and Wasson, 1993). Although the compositions of pyroxene-silica objects are similar to those predicted for pyroxene-silica cumulates, the drop-formed character and textures of many of them strongly imply that they originated as independent, suspended objects. Such objects may therefore have originated in a nebular setting, although the possibility that they formed as droplets by the remelting of differentiated material should be investigated.

Fayalite-silica objects generally appear to have irregular margins (Brigham *et al.*, 1986) and consist primarily of a silica mineral that is cross-cut and rimmed by fayalitic olivine (Fa_{57-96}); they also contain highly variable amounts of occasionally coarse, magnesian orthopyroxene (Brigham *et al.*, 1986; Krot and Wasson, 1993). Fayalitic olivine (>Fa_{59}) can exist in equilibrium with a silica polymorph but not also with orthopyroxene (Bowen and Schairer, 1935), requiring that the fayalite-silica objects that also contain orthopyroxene are in disequilibrium. These objects may represent pyroxene-silica objects (cumulates?) that were reacting with trapped or residual liquids, forming fayalite and decomposing orthopyroxene. In this case, both the pyroxene and silica grains would have existed before the formation of the fayalitic olivine, consistent with the apparent cross-cutting and rimming relationships. The fayalite veins would thus be analogous to the clinopyroxene rims and veins in Bo-1 tridymite, which appear to have formed by reaction between tridymite and residual liquid.

CONCLUSION

A large, igneous-textured clast of silica-rich orthopyroxenite in the Bovedy (L3) chondrite shows good evidence of having cooled from a siliceous, pyroxenitic melt. Cooling was fast enough to prevent complete equilibrium from being attained but slow enough to allow virtually all of the liquid to crystallize. The clast was probably derived from an asteroid or planetesimal that formed in the same region of space as ordinary chondrites. If the precursor was similar to ordinary chondrites, as seems likely, then the clast could be an igneous differentiate that experienced: (1) loss of essentially all metallic liquid at a temperature of 1335 ± 50 °C, and incomplete loss of silicate liquid at about the same time, during equilibrium partial melting; and (2) subsequent removal of most of the remaining metal, all of the remaining olivine, and some low-Ca pyroxene during melting at higher temperatures, with olivine separating from the precursor melt at the highest temperature and low-Ca pyroxene separating shortly afterwards. These fractionation events could have occurred in one melting episode if temperature

increased slowly prior to the removal of olivine, possibly as a result of heating by radionuclides or by electromagnetic induction. The clast may be a sample of a chemically and mineralogically stratified magma chamber that formed near the surface of the parent object. Other silica-rich objects in ordinary chondrites may also have formed in part through igneous differentiation.

Acknowledgements–The writers wish to thank Ronald Farrell for donating the piece of Bovedy with Bo-1 to the University of Arizona, and also Melinda Hutson, Yukio Ikeda, Addi Bischoff, and Hiroko Nagahara for constructive reviews of this manuscript. Special thanks are also extended to Y. Ikeda for pointing out the possible role of metastable crystallization in the crystallization of Bo-1 and the potential utility of the forsterite-nepheline-quartz phase diagram. This study was supported by NASA grant NAGW 3373 and NSF grant EAR 92-18857.

Editorial handling: H. Nagahara

REFERENCES

ANDERSEN O. (1915) The system anorthite-forsterite-silica. *Amer. Jour. Sci.* **39,** 407–454.

BISCHOFF A., METZLER K., STÖFFLER D., PALME H. AND SPETTEL B. (1989) Mineralogy and chemistry of the anomalous chondritic breccia ALH 85085 (abstract). *Lunar Planet. Sci.* **20,** 80–81.

BISCHOFF A. K., GEIGER T., PALME H., SPETTEL B., SCHULTZ L., SCHERER P., SCHLÜTER J. AND LKHAMSUREN J. (1993) Mineralogy, chemistry, and noble gas contents of Adzhi-Bogdo—an LL3-6 chondritic breccia with L-chondritic and granitoidal clasts. *Meteoritics* **28,** 570–578.

BOWEN N. L. AND SCHAIRER J. F. (1935) The system, MgO-FeO-SiO_2. *Amer. Jour. Sci.* **29,** 151–217.

BRIDGES J.C., FRANCHI I. A., HUTCHISON R. AND PILLINGER C. T. (1993) A new oxygen reservoir? Cristobalite-bearing clasts in Parnallee (abstract). *Meteoritics* **28,** 329–330.

BRIGHAM C. A., YABUKI H., OUYANG Z., MURRELL M. T., EL GORESY A. AND BURNETT D. S. (1986) Silica-bearing chondrules and clasts in ordinary chondrites. *Geochim. Cosmochim. Acta* **50,** 1655–1666.

CLAYTON R. N. AND KIEFFER S. W. (1991) Oxygen isotopic thermometer calibrations. In *Stable Isotope Geochemistry: A Tribute to Samuel Epstein* (eds. H. P. Taylor, J. R. O'Neil and I. R. Kaplan), pp. 3–10. Geochemical Society Special Publication, No. 3.

CLAYTON R. N., MAYEDA T. K., OLSEN E. J. AND PRINZ M. (1983) Oxygen isotope relationships in iron meteorites. *Earth Planet. Sci. Lett.* **65,** 229–232.

CLAYTON R. N., MAYEDA T. K., GOSWAMI J. N. AND OLSEN E. J. (1991) Oxygen isotope studies of ordinary chondrites. *Geochim. Cosmochim. Acta* **55,** 2317–2337.

DEER W. A., HOWIE R. A. AND ZUSSMAN J. (1966) *An Introduction to the Rock-forming Minerals.* Longman Group Ltd. 528 pp.

DODD R. T. (1978) Compositions of droplet chondrules in the Manych (L3) chondrite and the origin of chondrules. *Earth Planet. Sci. Lett.* **40,** 71–82.

DODD R. T. (1981) *Meteorites, A Petrologic-Chemical Synthesis.* Cambridge Univ. Press. 368 pp.

DODD R. T. AND JAROSEWICH E. (1976) Olivine microporphyry in the St. Mesmin chondrite. *Meteoritics* **11,** 1–20.

EHLMANN A. J., SCOTT E. R. D., KEIL K., MAYEDA T. K., CLAYTON R. N., WEBER H. W. AND SCHULTZ L. (1988) Origin of fragmental regolith breccias—evidence from the Kendleton L chondrite breccia. *Proc. Lunar Planet. Sci. Conf.* **18th,** 545–554.

FODOR R. V. AND KEIL K. (1976a) Carbonaceous and non-carbonaceous lithic fragments in the Plainview, Texas, chondrite: Origin and history. *Geochim. Cosmochim. Acta* **40,** 529–535.

FODOR R. V. AND KEIL K. (1976b) A komatiite-like lithic fragment with spinifex texture in the Eva meteorite: Origin from a supercooled impact melt of chondritic parentage. *Earth Planet. Sci. Lett.* **29,** 1–6.

GRAHAM A. L., EASTON A. J., HUTCHISON R. AND JEROME D. Y. (1976) The Bovedy meteorite: Mineral chemistry and origin of its Ca-rich glass inclusions. *Geochim. Cosmochim. Acta* **40,** 529–535.

GROSSMAN J. N., RUBIN A., NAGAHARA H. AND KING E. A. (1988) Properties of chondrules. In *Meteorites and the Early Solar System* (eds. J. F. Kerridge and M. S. Matthews), pp. 619–659. Univ. Arizona Press, Tucson, Arizona.

HANSEN M. AND ANDERKO K. (1958). *Constitution of Binary Alloys.* McGraw-Hill Book Company. 1305 pp.

HEWINS R. H. AND NEWSOM H. E. (1988) Igneous activity in the early solar system. In *Meteorites and the Early Solar System* (eds. J. F. Kerridge and

HILL H. (1993) Three unusual chondrules in the Bovedy (L3) chondrite (abstract). *Meteoritics* **28,** 363.

HUTCHISON R., WILLIAMS C. T., DIN V. K., CLAYTON R. N., KIRSCHBAUM C., PAUL R. L. AND LIPSCHUTZ M. E. (1988) A planetary, H-group pebble in the Barwell, L6, unshocked chondritic meteorite. *Earth Planet. Sci. Lett.* **90,** 105–118.

IRVING A. J. (1977) A review of experimental studies of crystal/liquid trace element partitioning. *Geochim. Cosmochim. Acta* **42,** 743–770.

JONES J. H. AND DRAKE M. J. (1986) Geochemical constraints on core formation in the Earth. *Nature* **322,** 221–228.

KALLEMEYN G. W., RUBIN A. E., WANG D. AND WASSON J. T. (1989) Ordinary chondrites: Bulk compositions, classification, lithophile-element fractionations, and composition-petrographic type relationships. *Geochim. Cosmochim. Acta* **53,** 2747–2767.

KEIL K., FODOR R. V., STARZYK P. M., SCHMITT R. A., BOGARD D. D. AND HUSAIN L. (1980) A 3.6-b.y.-old impact melt rock fragment in the Plainview chondrite: Implications for the age of the H-group chondrite parent body regolith formation. *Earth Planet. Sci. Lett.* **51,** 235–247.

KENNEDY A. K., HUTCHISON R., HUTCHEON I. D. AND AGRELL S. O. (1992) A unique high Mn/Fe microgabbro in the Parnallee (LL3) ordinary chondrite: Nebular mixture or planetary differentiate from a previously unrecognized planetary body? *Earth Planet. Sci. Lett.* **113,** 191–205.

KRING D. A. (1993) Cat Mountain: A meteoritic sample of an impact-melted chondritic asteroid (abstract). *Lunar Planet. Sci.* **24,** 823–824.

KROT A. N. AND WASSON J. T. (1993) Silica-fayalite bearing chondrules in ordinary chondrites: Evidence of oxidation in the solar nebula (abstract). *Meteoritics* **28,** 384.

LIPIN B. R. (1978) The system Mg_2SiO_4-Fe_2SiO_4-$CaAl_2Si_2O_8$-SiO_2 and the origin of Fra Mauro basalts. *Amer. Mineral.* **63,** 350–364.

MASON B. (1965) The chemical composition of olivine-bronzite and olivine-hypersthene chondrites. *Amer. Mus. Novitates,* No. 2223.

MASON B. (1966) The enstatite chondrites. *Geochim. Cosmochim. Acta* **30,** 23–39.

MASON B. (1971) *Handbook of Elemental Abundances in Meteorites.* Gordon and Breach Science Publishers. 555 pp.

MASUDA A., NAKAMURA N. AND TANAKA T. (1973) Fine structures of mutually normalized rare-earth patterns. *Geochim. Cosmochim. Acta* **37,** 239–248.

MCKAY G. A. (1986) Crystal-liquid partitioning of REE in basaltic systems: Extreme fractionation of REE in olivine. *Geochim. Cosmochim. Acta* **50,** 69–79.

MCKAY G. A. AND WEILL D. F. (1977) Petrogenesis of KREEP. *Proc. Lunar Planet. Sci. Conf.* **7th,** 2427–2447.

MCKAY G., WAGSTAFF J. AND LE L. (1991) REE distribution coefficients for pigeonite: Constraints on the origin of the mare basalt europium anomaly (abstract). *Lunar Planet. Sci.* **21,** 773–774.

MORSE S. A. (1980) *Basalts and Phase Diagrams.* Springer-Verlag. 493 pp.

NAKAMURA N., MISAWA K., KITAMURA M., MASUDA A., WATANABE S. AND YAMAMOTO K. (1990) Highly fractionated REE in the Hedjaz (L) chondrite: Implications for nebular and planetary processes. *Earth Planet. Sci. Lett.* **99,** 290–302.

OLSEN E. J. (1983) SiO_2-bearing chondrules in the Murchison (C2) meteorite. In *Chondrules and Their Origins* (ed. E. A. King), pp. 223–234. Lunar and Planetary Institute, Houston, Texas.

OLSEN E. AND JAROSEWICH E. (1970) The chemical composition of the silicate inclusions in the Weekeroo Station iron meteorite. *Earth Planet. Sci. Lett.* **8,** 261–266.

OLSEN E. J., MAYEDA T. K. AND CLAYTON R. N. (1981) Cristobalite-pyroxene in an L6 chondrite: Implications for metamorphism. *Earth Planet. Sci. Lett.* **56,** 82–88.

PHINNEY W. C. AND MORRISON D. A. (1990) Partition coefficients for calcic plagioclase: Implications for Archean anorthosites. *Geochim. Cosmochim. Acta* **54,** 1639–1654.

PLANNER H. N. (1983) Phase separation in a chondrule fragment from the Piancaldoli (LL3) chondrite. In *Chondrules and Their Origins* (ed. E. A. King), pp. 235–242. Lunar and Planetary Institute, Houston, Texas.

RUBIN A. E., KEIL K., TAYLOR G. J., MA M.-S., SCHMITT R. A. AND BOGARD D. D. (1981) Derivation of a heterogeneous lithic fragment in the Bovedy L-group chondrite from impact-melted porphyritic chondrules. *Geochim. Cosmochim. Acta* **45,** 2213–2228.

RUBIN A. E., JERDE E. A., ZONG P., WASSON J. T., WESTCOTT J. W., MAYEDA T. K. AND CLAYTON R. N. (1986) Properties of the Guin ungrouped iron meteorite: The origin of Guin and of group-IIE irons *Earth Planet. Sci. Lett.* **76,** 209–226.

RUZICKA A. AND BOYNTON W. V. (1992a) A distinctive silica-rich, sodium-poor igneous clast in the Bovedy (L3) chondrite (abstract). *Meteoritics* **27,** 283.

RUZICKA A. AND BOYNTON W. V. (1992b) The origin of silica-rich chondrules and clasts in ordinary and carbonaceous chondrites (abstract). *Meteoritics* **27,** 284.

RUZICKA A., KRING D. A., HILL D. H. AND BOYNTON W. V. (1993) The trace element composition of a silica-rich clast in the Bovedy (L3/4) chondrite (abstract). *Meteoritics* **28,** 426–427.

SCHAIRER J. F. AND YODER H. S., JR. (1961) Crystallization in the system nepheline-forsterite-silica at one atmosphere pressure. *Carnegie Inst. Wash. Yearbook 1960–1961*, 141–144.

STÖFFLER D., KEIL K. AND SCOTT E. R. D. (1991) Shock metamorphism of ordinary chondrites. *Geochim. Cosmochim. Acta* **55,** 3845–3867.

TAYLOR G. J., KEIL K., MCCOY T., HAACK H. AND SCOTT E. R. D. (1993) Asteroid differentiation: Pyroclastic volcanism to magma oceans. *Meteoritics* **28,** 34–52.

VILLEMANT B., JAFFREZIC H., JORON J.-L. AND TREUIL M. (1981) Distribution coefficients of major and trace elements: Fractional crystallization in the alkali basalt series of Chaîne des Puys (Massif Central, France). *Geochim. Cosmochim. Acta* **45,** 1997–2016.

WATSON E. B. (1977) Partitioning of manganese between forsterite and silicate liquid. *Geochim. Cosmochim. Acta* **41,** 1363–1374.

WEILL D. F. AND MCKAY G. A. (1975) The partitioning of Mg, Fe, Sr, Ce, Sm, Eu and Yb in lunar igneous systems and a possible origin of KREEP by equilibrium partial melting. *Proc. Lunar Planet. Sci. Conf.* **6th,** 1143–1158.

WLOTZKA F., PALME H., SPETTEL B., WÄNKE H., FREDRIKSSON K. AND NOONEN A. F. (1983) Alkali differentiation in LL-chondrites. *Geochim. Cosmochim. Acta* **47,** 743–757.

ZIEBOLD T. O. (1967) Precision and sensitivity in electron microprobe analysis. *Anal. Chem.* **39,** 858–861.